Research Article

Guo Kai*, He Miaohong, Pan Wenhao, and Wu Jinguo

Molecular dynamics of C-S-H production in graphene oxide environment

https://doi.org/10.1515/rams-2022-0007 received August 31, 2021; accepted November 14, 2021

Abstract: The process of calcium silicate hydrate (C-S-H) generation in graphene oxide (GO) nanoslits was investigated via molecular dynamics simulations using the structural polymerization reaction of silica chains in the synthesis of silica gels. The structural evolution of C-S-H, radial distribution functions, chemical components, and distribution of Q_n units in the system were analyzed to investigate the influence of GO on the early growth mechanism of C-S-H and compare the structural differences of C-S-H in the presence and absence of GO. The results showed that the proportion of silicon atoms bonded to bridge-site oxygen atoms in the C-S-H structure increased in the presence of oxygen-containing graphene groups. Ion adsorption in the GO surface layer led to an increase in the degree of polymerization of C-S-H. The nucleation and templating effects of GO were confirmed, revealing the intrinsic mechanism for the formation of GO-modified reinforced cementitious materials.

Keywords: molecular dynamics, calcium silicate hydrate, graphene oxide, polymerization reaction

1 Introduction

Calcium silicate hydrate (C–S–H), which is the main product of cement hydration – occupying more than 60% of the volume fraction – is the key component influencing the mechanical properties and durability of cement-based materials [1]. The development of nanotechnology in recent years has provided new approaches for the modification of

* Corresponding author: Guo Kai, School of Civil Engineering, Shenyang Jianzhu University, Shenyang 110168, China, e-mail: 43404844@qq.com

He Miaohong, Wu Jinguo: School of Civil Engineering, Shenyang Jianzhu University, Shenyang 110168, China

Pan Wenhao: School of Materials Science and Engineering, Shenyang Jianzhu University, Shenyang 110168, China cementitious materials. C-S-H gels are significantly complex in composition and structure, and are made up of basic units of calcium ions, namely, silicon-oxygen tetrahedron and water molecules [2]. The C-S-H generation process can be divided into two steps: dissolution of cement ions and bonding between ions to produce precipitation [3]. The polymerization reaction of the silicon chain structure is similar to the synthesis of silica sol-gel oxide, and the most important chemical reaction is the polymerization between silicon hydroxyl groups [4]. The increase in polymerization of the Si(OH)4 system can be characterized by the bonding state and ratio of the O and Si atoms present, and the local network of Si atoms determines the kinetics of the polymerization reaction [5]. Graphene Oxide (GO) is a functionalized derivative of graphene [6]. GO has a large specific surface area, excellent mechanical properties, and good water solubility [7]. It contains numerous reactive functional groups, such as hydroxyl (-OH) and epoxy groups (-O-), making it a popular cement-based modifier [8]. Numerous experimental results demonstrate that the incorporation of GO promotes the hydration of cement and increases the density of the hydration products, thus improving the tensile and flexural properties as well as the durability of cementitious materials [9].

Although GO has been effective in improving the macro-mechanical properties of cementitious materials, the modification mechanism is not yet clear, and therefore, practical engineering applications for GO-modified cementitious materials are limited [10]. The influence of nanomaterials on the morphological characteristics of hydrated crystals and ionic interactions at the nanoscale cannot be accurately characterized experimentally owing to the limitations of instrumentation and current measurement techniques. Molecular dynamics simulation is a numerical calculation method based on force fields, enabling the prediction of structural and dynamic properties of hydrated molecules at the atomic and molecular scales; it is one of the best techniques for the microscopic simulation of materials [11]. With the development and advancement of computer technology, molecular simulation techniques have been increasingly used in the development of new cement-based materials. Using this approach,

researchers have conducted molecular dynamics simulations of the hydration process of cement by nanomaterials such as GO [12]. The effect of GO on the formation of hydration products has been investigated using reactive molecular dynamics simulations, and C–S–H and GO interface models have been established to study the interaction between GO surfaces with different functional groups and C–S–H gel surfaces [13]. In addition, the atomic-to-continuum framework is used to extract dynamic trends when appropriate models for incorporating non-periodic and anisotropic electric fields into molecular dynamics simulations are lacking. This provides the mathematical and algorithmic infrastructure to couple finite element (FE) representations of continuous data with atomic data [14].

Current studies on GO-enhanced modified cementitious materials based on molecular dynamics are more concerned with the action of a small number of molecules and various types of oxygen-containing groups and interfacial properties with a single applicable force field. Moreover, the studied systems are small and do not include kinetic simulation studies of the reaction processes that actually form hydration products. However, oxygen content is one of the more important performance parameters of GO, and very few simulation studies have considered this factor.

To address the shortcomings of the existing research and meet the urgent demand to develop engineering applications for GO-modified cementitious materials, this study adopts a molecular dynamics approach to construct GO nanoslits and investigates the early C–S–H generation process by simulating the silicon oxide gel formation process. By comparing the effect of the presence and absence of GO, the oxygen atom content at bridge sites, local connectivity of Si atoms, and atom pair radial distribution function (RDF) in the C–S–H model were investigated to reveal the mechanism by which the GO environment initiates and sustains C–S–H polymerization.

2 Model construction and simulation methods

2.1 Principles of molecular dynamics

When a simulated system contains more than one molecule or atom, the energy of the system includes the sum of the total kinetic energy and total potential energy of all the atoms. The total potential energy, U, is a function of the position of the individual atoms. Specifically, it can be

subdivided into two main components: the non-bonded van der Waals interaction between atoms, U_{vdw} , and the intramolecular potential energy, U_{int} . Specifically,

$$U = U_{\text{vdw}} + U_{\text{int}}, \tag{1}$$

 U_{vdw} can be approximated as the sum of the van der Waals interactions between pairs of atoms, whereas U_{int} is the sum of the potential energies for each type of coordinate (bond length stretching energy and bond angle bending energy). According to classical mechanics, the force F on any atom i is the gradient of the potential energy, and the acceleration of the atom is

$$\overrightarrow{a_i} = \frac{\overrightarrow{F_i}}{m_i}. (2)$$

By integrating Newton's equations of motion with respect to time, the velocity and position of atom i after time t can be obtained:

$$\overrightarrow{v_i} = \overrightarrow{v_i}^0 + \overrightarrow{a_i}t, \tag{3}$$

$$\overrightarrow{r_i} = \overrightarrow{r_i}^0 + \overrightarrow{v_i}t + \frac{1}{2}\overrightarrow{a_i}t^2, \tag{4}$$

where $\overrightarrow{r_i}$ represents the position of atom i, $\overrightarrow{v_i}$ represents the velocity of atom i, the superscript 0 represents the initial moment, and t represents the moment. With $t = \delta t$ representing a very short time interval, the position and velocity of the ith atom after the interval δt can be calculated. The acceleration at this point is then recalculated according to the new position, and the position and velocity at the next moment are then recalculated to obtain information on the position and velocity of all atoms in the system as a function of time.

2.2 Model building

The early generation of C–S–H was studied using reaction molecular dynamics with reference to the simulation of the silica oxide gel process [15]. During the polymerization reaction, the main components of silica oxide colloids, namely C_3S and C_2S , are hydrolyzed to $Si(OH)_4$, which then undergoes polymerization aging [16]. To simplify the reaction process, $Si(OH)_4$ molecules were added directly to the simulation. Considering the model size effect and computational limitations, the number of $Si(OH)_4$ molecules was determined to be 6^3 , i.e., 216; $H_2O/Si = 3$ based on the influence of H_2O on the polymerization rate [17]. The calcium:silica ratio of C-S-H produced after the hydration reaction was 1.75 on average, and combined with the active energy of C-S-H and its

Table 1: Model system components and related parameters

Model	Number of molecules			Spacing	Oxygen
	Si(OH) ₄	Ca(OH) ₂	H ₂ O	of slits/Å	content of GO (%)
Control	216	324	648	40	_
GCOOH40-25	216	324	648	40	25
GCOOH40-50	216	324	648	40	50
GCOOH10-25	216	324	648	10	25

thermodynamic stability, the simulated Ca:Si ratio was determined to be 1.5 [18].

The simulations were performed in large-scale atomic/molecular massively parallel simulator (LAMMPS; Sandia

National Laboratories) with a reactive force field (ReaxFF), and the trajectories of the atoms were calculated using the Verlet algorithm with a time step of 0.25 fs [19]. The parameters of the ReaxFF were derived from a fit to quantum calculations [20]. First, the model was simulated kinetically using a regular system synthesis (NVT) so that the initial system was chilled for 100 ps at 300 K. The system was then chilled for 500 ps at 300 K and 0 pressure in an isothermal isobaric system (NPT). After two chilling processes, the architecture was optimized, and a steady state condition of energy and volume was achieved [21]. A temperature of 2,000 K was used to keep the model reacting at a constant temperature under NVT synthesis, and the number of simulation steps was set to 2,000,000 with a total duration of 500 ps. Finally, the simulation was

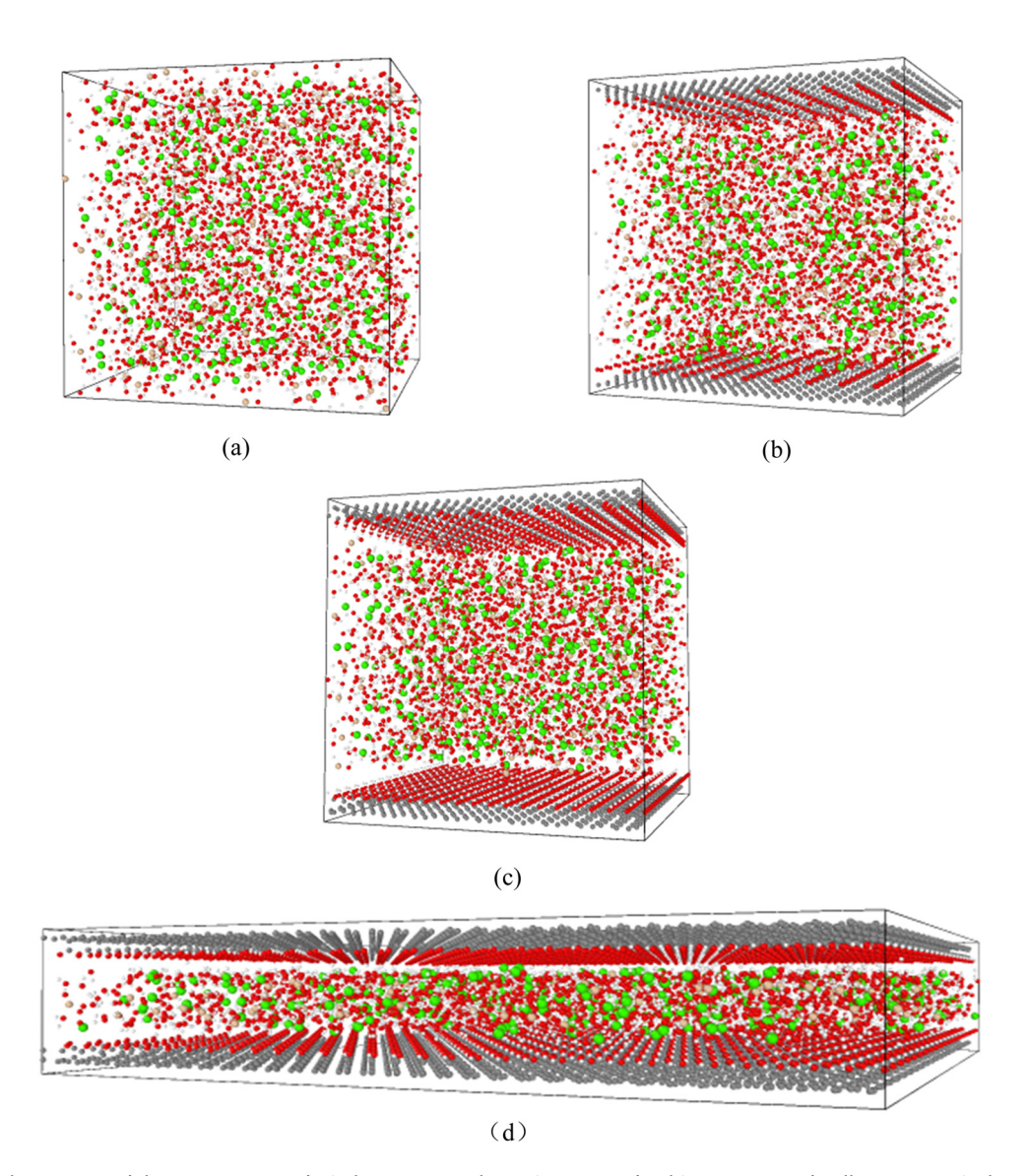


Figure 1: Initial system model (C, O, H, Ca, and Si elements are shown in gray, red, white, green, and yellow, respectively). (a) Control, (b) GCOOH40-25, (c) GCOOH40-50, and (d) GCOOH10-25.

concluded by gradually cooling the gel-generating system to 300 K and chilling it for 100 ps under NPT system conditions at 0 pressure to obtain C–S–H.

The initial model of graphene was derived from the graphite crystal of the system, and a graphene sheet layer with a = 39.36 Å and b = 39.36 Å was obtained by replication in the x and y directions; a carboxyl group (-COOH) was added to the graphene surface to form a GO sheet layer [22]. Two types of GO sheet layer with 25 and 50% oxygen content were simulated and constructed to study the effects of different oxygen contents of GO on the cementitious materials. Slits with different spacing of 40 and 10 Å were constructed to study the effect of different doping amounts of GO. The same simulation procedure and system parameters were used to obtain early

C–S–H gel crystal models by placing molecular reactant solutions that are consistent with the above model into different GO sheet layers and different spacing slits [23]. The model construction parameters are listed in Table 1, and the initial system model is shown in Figure 1.

3 Results and analysis

After reaction aging, the presence of siloxane chains and ring structures within each system can be observed as shown in Figure 2, indicating the generation of early C–S–H crystal structures [24]. The different systems can be compared by performing a detailed analysis of the relevant parameters within the systems.

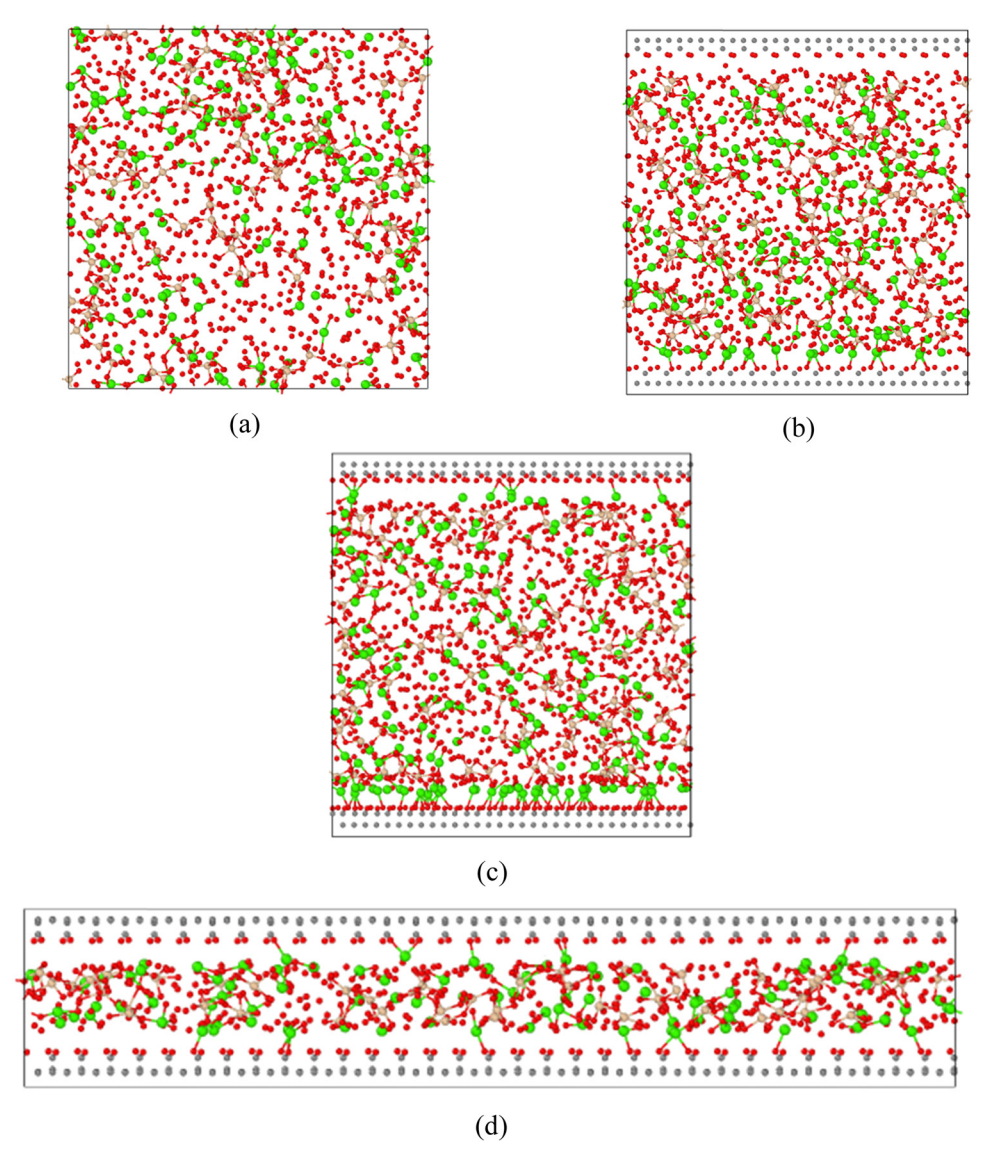


Figure 2: Atomic configurations of C-S-H. (a) Control, (b) GCOOH40-25, (c) GCOOH40-50, and (d) GCOOH10-25.

94

3.1 Structural evolution of C-S-H

First, the changes in the reactions involving oxygen and silicon atoms in the models were investigated to compare the differences in the early C-S-H crystal structures in the different system models. The number of bridging oxygen atoms (BO, i.e., one oxygen atom linked to two silicon atoms) in the structure and those of non-bridging oxygen atoms (NBO, i.e., oxygen atoms linked to only one silicon atom) can be calculated by determining the number of partial coordination sites per atom [24]. The overall degree of polymerization in silicon oxide chain-structured colloids can be represented by the ratio of bridging oxygen atoms to silicon atoms (BO/Si), and the reaction rate of polymerization can be obtained from the BO/Si curve with time [25]. As shown in Figure 3, the ratio of BO to Si increased with an increase in the reaction time, reflecting a continuous increase in the overall polymerization of the system, which gradually stabilized in the later stages of the aging reaction [26]. A comparison of the variation curves of the groups indicates that the GO-free reference group started the reaction with a BO number of 0. The reaction process was stable and equilibrium was achieved in a very short time. In the model with the GO slit, a small amount of BO was formed at the end of the chilling process and the BO/Si ratio was approximately 0.1 at the beginning of the reaction, which also indicates that the C-S-H polymerization barrier was lowered and the chain structure was more easily formed under the effect of the site resistance of the nanoslit. Figure 4 represents the final content of BO at the bridge position. The GCOOH40-25 and GCOOH40-50 systems formed the highest amount of BO, with a BO/Si ratio of approximately 0.6. In contrast, GCOOH10-25 formed the least amount of BO and the BO/Si ratio was only 0.28. which is the lowest of all the systems. The initial slope of the BO/Si content curve corresponds to the polymerization rate

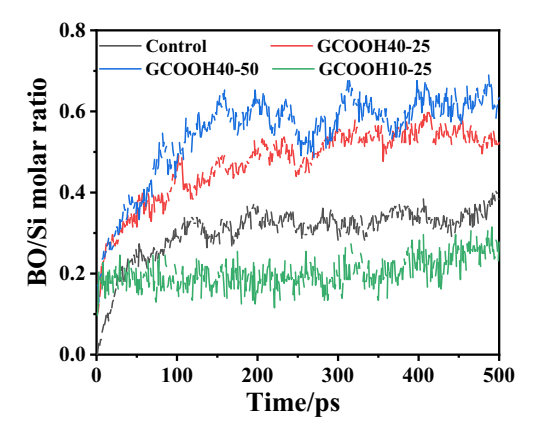


Figure 3: Variation curves of Bo/Si for the different systems.

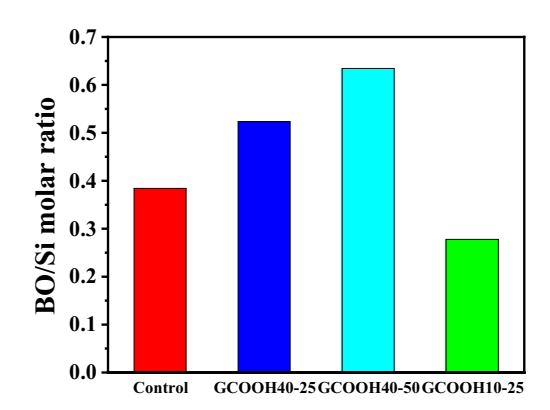


Figure 4: Final bridging oxygen atom content.

of the aging reaction, which is closer to the GCOOH40-25 and GCOOH40-50 reaction rates in the early comparison group. The modulating effect of the nanoslits in the middle of the reaction allows the polymerization reaction to continue, with higher amounts of BO formed.

The silicon atoms were classified into Q_0 – Q_4 by counting the number of silicon atoms bonded to BO. The change curve of Q_n in each system is shown in Figure 5, whereas the final Q_n content distribution is shown in Figure 6. It can be observed that the reference group only contained Q_0 at the beginning of the reaction, whereas Q_1 , Q_2 , and a small amount of Q_3 were gradually formed in subsequent reactions. In the GO slit system, a small amount of Q_1 was already present at the beginning of the reaction, as in the case of BO. The number of Q_1 units in the GCOOH40-25 and GCOOH40-50 systems increased rapidly as the reaction proceeded and decreased after reaching peak values, whereas the number of Q_2 and Q_3 units increased, indicating that the silica atoms are more likely to produce highly polymerized unit structures in the GO environment [27]. Ultimately, Q_2 and Q_3 units stabilized at 19.5 and 6.5% and 23.6 and 8.8%, respectively, which were much higher than those of the reference group. Furthermore, some Q_4 units were produced in both the systems. In the GCOOH10-25 system, the number of Q_1-Q_3 units was the lowest of all systems, and that of Q_4 units was almost zero, as in the reference group.

A comprehensive comparison of the structural evolution of the early C–S–H crystal-formation process in each system indicates that the systems in the GO slit environment formed a certain number of chain structures in the chirality phase before the start of the reaction because of the site-blocking effect of the GO lamellae and the influence of the reactive oxygen-containing groups. During the reaction, the reaction rate in the system did not change significantly when the slit length was 40 Å. However, the number of silicon atoms in the Q_1 unit increased rapidly early in the reaction process and then decreased. The total

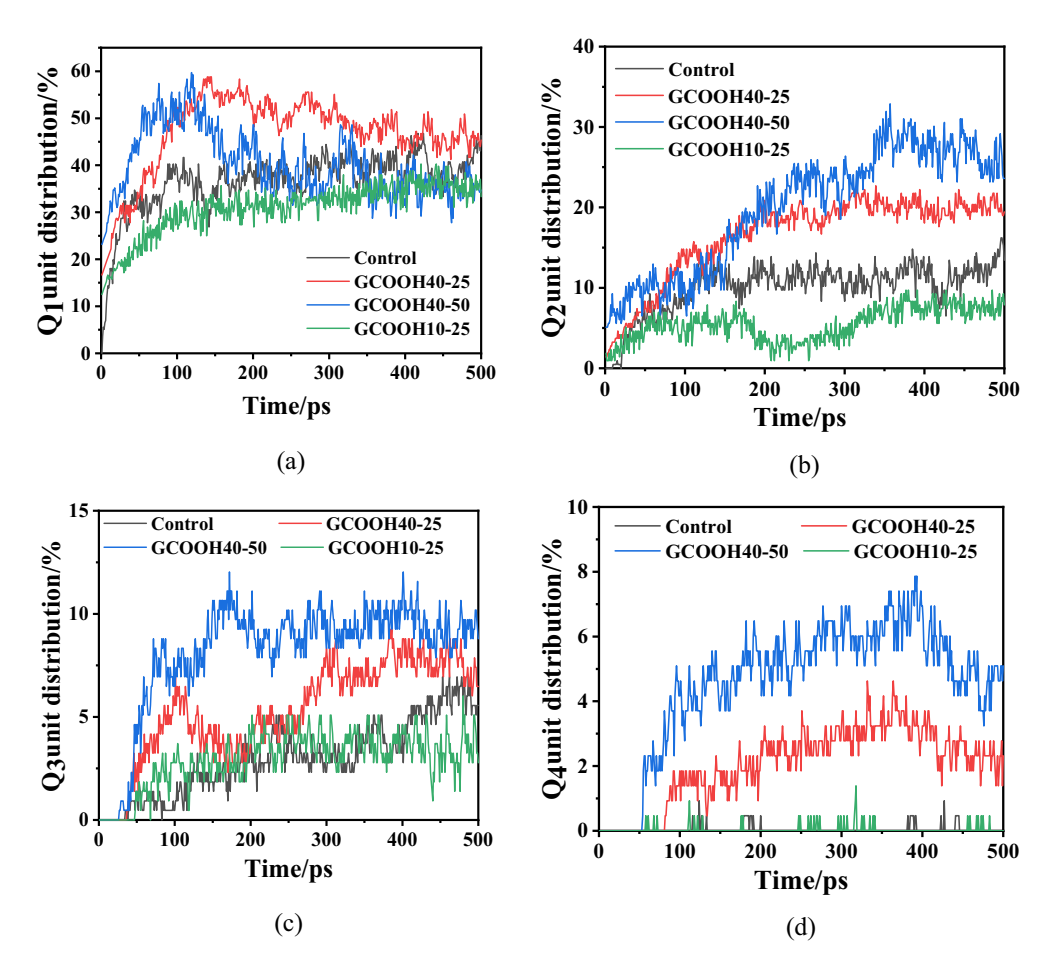


Figure 5: Variation curves of Q_n content. (a) Q_1 , (b) Q_2 , (c) Q_3 , and (d) Q_4 .

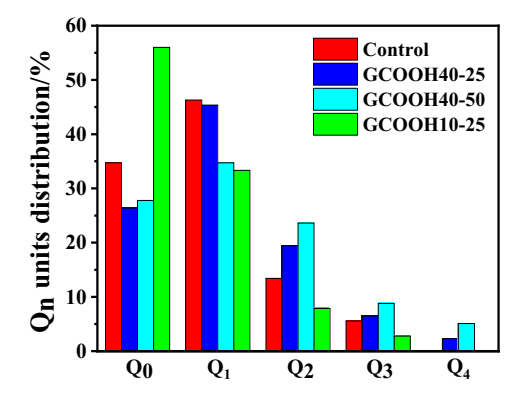


Figure 6: Distribution of Q_n content in each system.

number was essentially the same as the reference group when the reaction reached equilibrium, whereas the number of BO and number of silicon atoms in the Q_2 and Q_3 units increased significantly; a significant portion of Q_4 units was produced, indicating that the molecular structure tended to converge in the GO environment with a slit of 40 Å, and the overall polymerization of the system increased effectively.

A comparison of the content change curves of GCOOH40-25 and GCOOH40-50 indicates that under the same slit spacing conditions, the effect of 50% oxygenated GO lamellae on the system was slightly higher in the high polymerization units, such as BO quantity, Q_3 , and Q_4 than in the 25% oxygenated GO system, although the difference between the two is not significant. This indicates that in the simulation, GO oxygenation affects the structure of C–S–H in the system evolution, and the chain structure is more easily polymerized in the GO environment with high oxygen content [28].

When the slit distance was set to 10 Å, a comparison of the model curves shows that although the chain structure was generated during the initial stages, the system reached equilibrium in a very short time as the reaction proceeded; the BO content and Q_2 and Q_3 units were all significantly lower than in the simulated system at 40 Å, and lower than in the reference group without GO. The proportion of Q_0 units in the final Q_n unit distribution was more than 55%, i.e., more silicon atoms did not polymerize effectively, and the proportion of Q_1 units with low polymerization was much higher than the other units

in the Q_{1-4} units, indicating that even if polymerization did occur, it was only a short-range chain structure of a small size, with the lowest overall polymerization performance. This suggests that excessive GO doping and a nanoslit that is too small will restrict the reaction space in the solution and affect the full reaction of the molecules, preventing the C–S–H from early polymerizing effectively.

3.2 Analysis of the RDF

The RDF is a function representing the change in the density of a target particle within a certain distance from a reference atom. This function can reflect the change in the odds (g(r)) of a particular particle appearing within a certain range of any atom in the model and the arrangement, and is a common method of analysis in molecular dynamics [29]. The RDFs obtained through X-ray smallangle diffraction tests are mutually Fourier-dependent

and can be analyzed against simulation and test results [30].

By analyzing the final C-S-H model obtained for each group, the RDFs for the four types of atomic pairs, namely, Si-O, Si-Si, Ca-O, and Ca-Ca, can be calculated, as shown in Figure 7. It can be observed from Figure 7a that the Si-O bond function curves for all the models show a peak point at 1.6 Å, but the peak intensities are significantly different. The peak of the 40 Å slit model shows a significant increase compared with the control group, whereas that for the GCOOH40-50 model is slightly higher than that for GCOOH40-25. The GCOOH10-25 peak point is the lowest, and the differences in the other groups are more pronounced, indicating that the number of Si and O atoms bonded in the model increased and the density increased significantly in the GO environment with a slit of 40 Å. However, the Si-O bonding decreased with a slit of 10 Å. The steamed bun peak at 4 Å of the function curve corresponds to the non-bonded Si and O atoms in the model system. The peak magnitudes did not differ significantly between the models, with the GCOOH10-25 model,

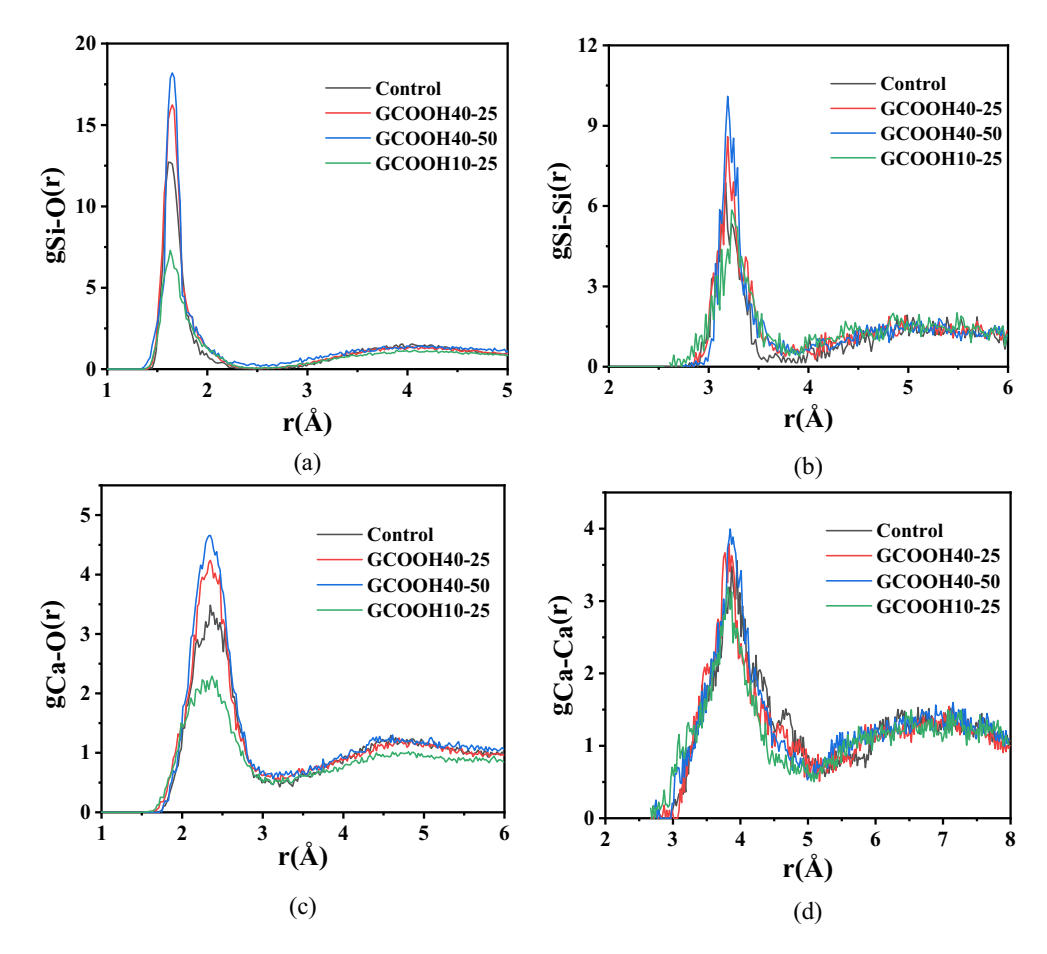


Figure 7: Atomic radial distribution function. (a) Si-O, (b) Si-Si, (c) Ca-O, and (d) Ca-Ca.

DE GRUYTER

which has a lower aggregation ratio, exhibiting a relatively small peak. Figure 7b shows the RDF of Si-Si. The Si atoms are linked to each other by bridge-site oxygen atoms, and the main peak of the curve occurs at 3.2 Å. The peak intensities of the GCOOH40-50 and GCOOH40-25 models are significantly higher than those of the other two curves, whereas the peak of GCOOH10-25 is closer to that of the reference group. This indicates that the polymerization of Si atoms is effectively enhanced by the increase in the oxygen atoms in the bridge position under the effect of nano-GO. The Si-Si function curve shows a bun peak at 5 Å. The peaks of the curves are still relatively close to each other, and the values for the GCOOH10-25 group are, in contrast, slightly higher. It can be inferred from the Q_n distribution that this may be related to the uneven dispersion of Si atoms when the slit is too small, and the lack of bonding of the locally concentrated Si atoms causes the Si-Si function curve to yield a higher intensity at the bun peak. Figure 7c shows the RDF of Ca-O. The high degree of polymerization of the GCOOH40-50 and GCOOH40-25 models results in a higher peak at 2.4 Å compared with

the other two groups, with a significant increase in the Ca–O bond density. It can be observed from the Ca–Ca RDF curve in Figure 7d that the GCOOH10-25 model has a lower intensity in the Ca–O function curve; however, the intensity of the main Ca–Ca peak is closer to those of the other models, indicating that the effect of GO still resulted in significant aggregation of Ca atoms in the solution even at low polymerization levels.

3.3 Distribution of chemical components

The distribution of Ca and Si atoms in the model in the z-axis was determined as shown in Figure 8, allowing the differences in the C–S–H density generated in the model system to be analyzed. A comparison of the distribution curves of Ca and Si in the reference group is shown in Figure 8a; it indicates that the atoms are more evenly distributed in the z-axis, and the Ca/Si ratio at each position remains essentially the same (1.5) in the initial

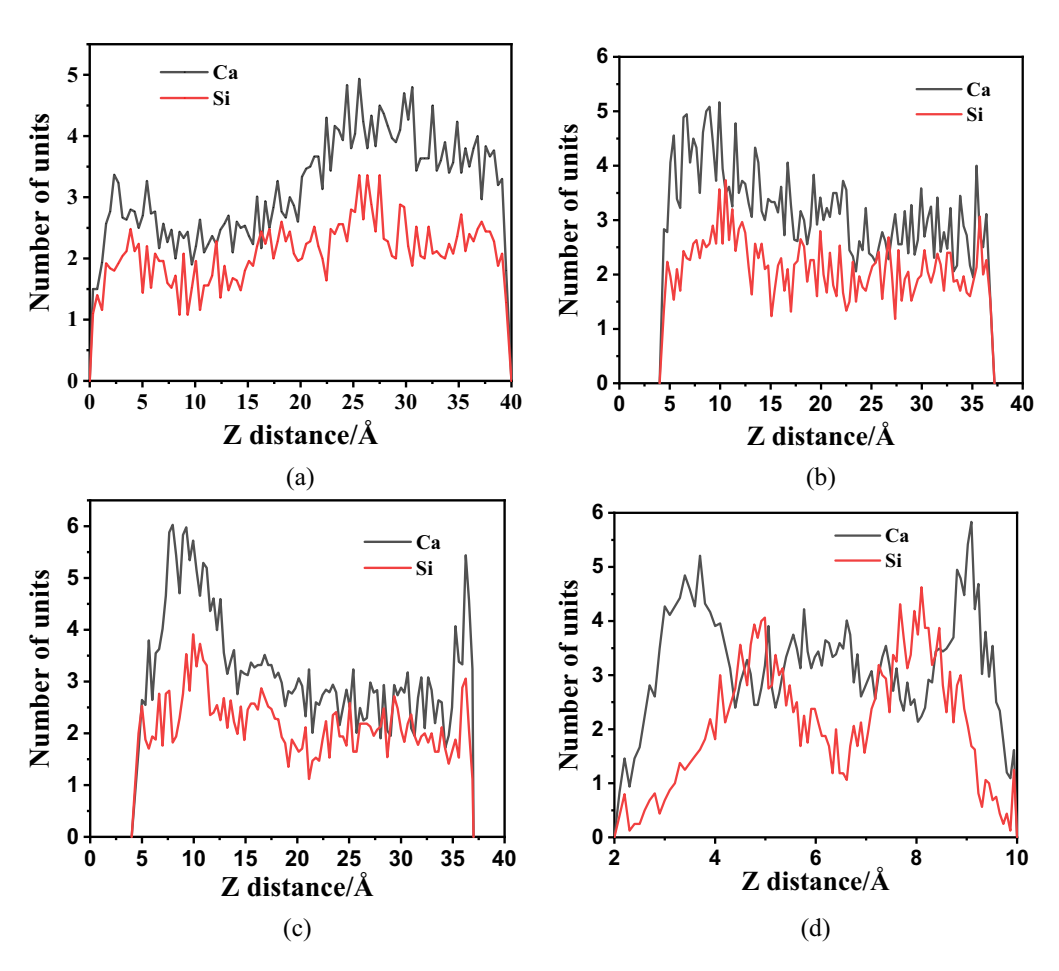


Figure 8: Distribution of Ca and Si atoms in z direction. (a) Control, (b) GCOOH40-25, (c) GCOOH40-50, and (d) GCOOH10-25.

system, with a peak in the number of atoms distributed in the middle of 25–30 Å range. This region is the C-S-H enriched region, which indicates that the C-S-H generated in the system tends to aggregate and form local clusters. Because there is a GO lamella of approximately 3 Å in the GCOOH40-25 model, the peaks of the distribution curves of Ca and Si in the 4-37 Å z-axis range in Figure 8b show a clear shift toward one side of the GO lamella, with the enriched region of Ca atom distribution appearing in the z-axis range of 7–12 Å, and the enriched region of Si atoms in the 10-13 Å range. This indicates that GO has an adsorption effect on both Ca and Si atoms. The adsorption of Ca atoms is more obvious. The distribution curves of Ca and Si for GCOOH40-50 in Figure 8c are more similar to the GCOOH40-25 model, whereas the peak number of Ca atoms further increases, creating a region of higher Ca/Si ratio locally. It can be concluded that the oxygen atoms in GO can effectively adsorb Ca and Si atomic groups, and the higher the amount of oxygen contained, the better the adsorption effect. Simulations of C-S-H gel polymerization with different Ca/Si

ratios show that the C-S-H production potential varies with different Ca/Si ratios, with the enthalpy of C-S-H production decreasing as this ratio increases, whereas the activation energy decreases and then increases as the ratio increases, reaching a minimum at a ratio of 1.8 [31]. At this point, if the number of Ca atoms continues to increase, more NBOs are induced within the system, decreasing the overall polymerization of the colloid [32]. Therefore, the enrichment of suitable Ca atoms in the GO-containing model increases the local Ca/Si ratio of the system [33], at which Ca atoms catalyze the early gel polymerization reaction and act to isolate the nano-space, thereby allowing the enrichment of Si(OH)₄ monomers, increasing the chance of collision, and increasing the rate of polymerization [33]. It can be observed from the Ca and Si distribution curves of GCOOH10-25 in Figure 8d that when the GO slit was too small, there was a non-uniform distribution of atoms in the system, with Ca atoms enriched at 3.8 and 9.2 Å and Si atoms enriched at 5 and 8 Å. The Ca/Si ratio varied significantly in different regions, resulting in the lowest degree of C-S-H polymerization.

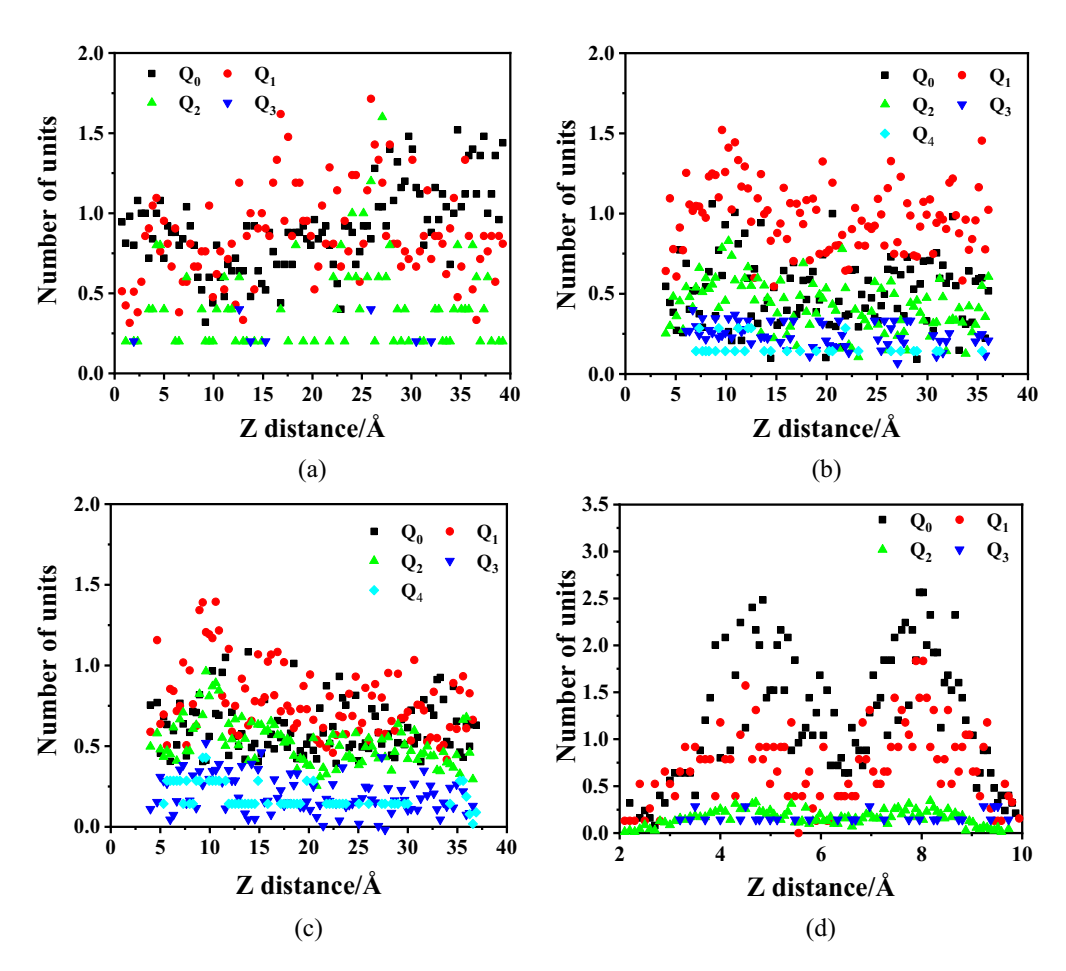


Figure 9: Q_n element distribution in z direction. (a) Control, (b) GCOOH40-25, (c) GCOOH40-50, and (d) GCOOH10-25.

3.4 Distribution of Q_n

The atomic structure of the gel largely determines the chemical composition of C-S-H; therefore, by exploring the distribution of Q_n units along the z-axis, it is possible to characterize the structural changes of C-S-H in the system. Figure 9a shows the distribution of Q_n units in the control group. It can be observed that the Q_1 and Q_2 units appear to aggregate in larger numbers around 25 Å, whereas the Q_3 units are fewer and randomly distributed, indicating that C-S-H is mostly a short-chain structure with clear convergence locations. There are also more Q_0 units in the system, indicating that the system contains C-H. This demonstrates that the early C-S-H system had a low degree of polymerization and the system was not homogeneous. Figure 9b shows the distribution of Q_n units in the GCOOH40-25 model, where the Q_0 units are reduced compared with the reference group. The overall distribution of Q_1 units is relatively homogeneous with a slight increase in number at 10 Å; more Q_2 and Q_3 units are aggregated at this position, which is consistent with the silica-rich region in Figure 8b, indicating that the highly linked C-S-H structure is likely to occur in the calcium-rich region with a high Ca/Si ratio. The presence of Q_4 units in the system, however, indicates that GO enhanced early C-S-H aggregation. Figure 9c shows the distribution of Q_n units in the GCOOH40-50 model. Similar to the GCOOH40-25 model, the number of O_1 units is further reduced, and Q_2 , Q_3 , and Q_4 units all exhibited content peaks at 8–10 Å. The system is more polymerized and has more highly linked structures. In the GCOOH10-25 model shown in Figure 9d, the Q_n unit content distribution appears quite different from the other systems and essentially maintains a high consistency with the Si atom distribution in Figure 8d, with Q_0 and Q_1 units obviously converging at 4.5 and 8 Å, respectively. The atomic uniformity of the system is poor, and the Q_2 unit content is already very low, with no Q_4 units generated.

The above analysis shows that when the GO slit spacing is moderate, i.e., when the GO doping amount is ideal, the adsorption and limiting effect of GO lamellae can effectively improve the polymerization of C–S–H and facilitate early C–S–H production. However, when the GO slit spacing is too small, i.e., when GO addition is significantly increased, the polymerization of C–S–H shows a significant weakening, which is consistent with the results of macroscopic tests where adding too much nanomaterial does not contribute to further improvement in the properties of the cementitious materials [34]. In most cases, this is due to the agglomeration effect of the nanomaterials, similar to macro-fiber addition, where there is a small

area of entanglement and aggregation in the area of excessive fiber density at high addition levels [35]. In this area, the transition zone between the cement paste and the fibers is dense, whereas the anchoring effect of the paste on the fibers is weakened and the bridging effect of the fibers is not present, such that this area within the matrix becomes weak and less durable. Therefore, the material admixture is also usually too high, resulting in difficult or uneven dispersion, which is the main reason for the poor modification effect [36].

In addition to the agglomeration effect described above, doping by GO has another effect based on the analysis of molecular reaction process simulations. When the slit is set to 10 Å, the Ca and Si distribution curves appear significantly different, with Ca atoms aggregating in response to GO; however, the Ca/Si ratios in different regions demonstrate strong randomness. This resulted in the system reaching equilibrium in a very short time, although the chain structure was generated earlier in the early stage of the aging process with a high content of monomeric Q_1 units, whereas the BO, Q_2 , and Q_3 units all had a low content, and essentially no Q_4 units with high polymerization were formed. Moreover, the products in the system were mostly shortrange chain structures of a small size, with extremely low overall polymerization performance. This indicates that when GO addition is high, the spacing between the nanolayers is too small and the difference in the adsorption of ions by GO during the hydration process becomes more obvious. This limiting effect also causes the ions within the lamellae to accumulate and not move sufficiently, resulting in a lower overall polymerization of C-S-H. This microscopic fragmentation effect tends to break up and unitize the gel, reducing the overall strength of the material. In other words, when the amount of nanomaterials added is too high, even if there is no agglomeration and the dispersion effect is extremely homogeneous, this fragmentation effect may become more obvious, resulting in poor modification of the composite material.

4 Conclusion

In this study, the early C–S–H generation process was investigated using a reaction molecular dynamics approach based on simulations of the silica oxide gel process. The effects of GO on the C–S–H generation process and on structural changes in a confined space at the nanoscale were simulated by adding GO sheets with different slits on both sides of the reaction system. The main conclusions are as follows.

- (1) Molecular dynamics simulations of the reaction can reflect the early C-S-H production process more accurately, and the complete early C-S-H structure is also obtained by placing the system in a nano-GO environment.
- (2) In the nano-GO environment, when the GO slit spacing is moderate, i.e., the GO doping amount is ideal, the domain-limiting effect of GO increases the probability of atomic collisions in the system and the oxygen-containing groups in GO can adsorb Ca and Si atoms, forming localized areas rich in Ca and Si, lowering the potential barrier for C–S–H formation, and improving the polymerization of the system. The adsorption effect of GO on Ca and Si atoms is related to the number of oxygen-containing groups, and the higher the oxygen content, the more pronounced the adsorption effect and the higher the C–S–H integrality.
- (3) When the spacing between GO slits is too small, i.e., when GO addition is increased significantly, the spatial limitation causes the atoms in the system to be unevenly dispersed, resulting in an inadequate overall reaction and a reduction in the degree of C–S–H polymerization. When the GO lamella spacing is too dense, the fragmentation effect occurs at the macroscopic scale, causing the gel to fragment and unitize. This effect becomes more pronounced at higher GO doping levels where GO is more uniformly dispersed, deteriorating the modification effect.

Acknowledgment: The author would like to acknowledge the support of Liaoning Provincial Education Department Scientific Research Project (LJKZ0565).

Funding information: Project molecular dynamics of C–S–H production in graphene oxide environment supported by Liaoning Provincial Education Department Scientific Research Project (LJKZ0565).

Author contribution: All the authors have accepted responsibility for the entire content of this submitted manuscript and approved submission.

Conflict of interest: The authors declare no conflicts of interest regarding this article.

References

Mehta, P. K. Concrete: microstructure, properties, and materials. *Preticehall International*, Vol. 13, No. 4, 2006, pp. 499–499.

- [2] Mehta, P. K. and P. J. M. Monteiro. Concrete: microstructure, properties, and materials, McGraw-Hill Education, New York, NY, 2014.
- [3] Allen, A. J., J. J. Thomas, and H. M. Jennings. Composition and density of nanoscale calcium-silicate-hydrate in cement. *Nature Materials*, Vol. 6, No. 4, 2007, pp. 311–316.
- [4] Richardson, I. G. The calcium silicate hydrates. Cement and Concrete Research, Vol. 38, No. 2, 2008, pp. 137-158.
- [5] Gao, W. The chemistry of graphene oxide. Graphene oxide, Springer, Berlin, Germany, 2015, pp. 61–95.
- [6] Ansari, P., J. Azamat, and A. Khataee. Computational study on the removal of trihalomethanes from water using functionalized graphene oxide membranes. *Chemical Physics*, Vol. 531, 2020, p. 110589.
- [7] Pakdel, S., S. Majidi, H. Erfan-Niya, and J. Azamat. *Graphene oxide and reduced graphene oxide as nanofillers in membrane separation*[M]/Two-Dimensional (2D) Nanomaterials in Separation Science, Springer, Cham, 2021, pp. 113–144.
- [8] Wang, J., Y. Xu, X. Wu, P. Zhang, and S. Hu. Advances of graphene- and graphene oxide-modified cementitious materials. *Nanotechnology Reviews*, Vol. 9, No. 1, 2020, pp. 465–477.
- [9] Liu, C., X. Huang, Y. Y. Wu, X. Deng, Z. Zheng, Z. Xu, et al. Advance on the dispersion treatment of graphene oxide and the graphene oxide modified cement-based materials. *Nanotechnology Reviews*, Vol. 10, No. 1, 2021, pp. 34–49.
- [10] Guo, K., H. Miao, and J. H. Zhou. Effect of graphene oxide on gas permeability of recycle concrete. *Journal of Shenyang Jianzhu University* (*Natural Science*), Vol. 35, No. 4, 2019, pp. 692–698.
- [11] Chen, Z. L., W. R. Xu, and L. D. Tang. Theory and practice of molecular simulation, Chemical Industry Press, Beijing, 2007.
- [12] Du, T., H. Li, G. Sant, and M. Bauchy. New insights into the sol-gel condensation of silica by reactive molecular dynamics simulations. *Journal of Chemical Physics*, Vol. 148, No. 23, 2018, pp. 234–254.
- [13] Sanchez, F. and L. Zhang. Molecular dynamics modeling of the interface between surface functionalized graphitic structures and calcium-silicate-hydrate: Interaction energies, structure, and dynamics. *Journal of Colloid Interface Science*, Vol. 323, No. 2, 2008, pp. 349-358.
- [14] Templeton, J. A., R. E. Jones, J. W. Lee, J. A. Zimmerman, and B. M. Wong. A long-range electric field solver for molecular dynamics based on atomistic-to-continuum modeling. *Journal* of Chemical Theory & Computation, Vol. 7, No. 6, 2011, pp. 1736–1749.
- [15] Qomi, M. A., K. J. Krakowiak, M. Bauchy, K. L. Stewart, R. Shahsavari, D. Jagannathan, et al. Combinatorial molecular optimization of cement hydrates. *Nature communications*, Vol. 5, No. 1, 2014, pp. 1–10.
- [16] Côté, A. S., A. N. Cormack, and A. Tilocca. Influence of calcium on the initial stages of the sol-gel synthesis of bioactive glasses. *The Journal of Physical Chemistry B*, Vol. 120, No. 45, 2016, pp. 11773–11780.
- [17] Ma, B. Y., T. J. Yang, and C. J. Pan. Simulation study on the interfacial properties of graphene oxide modified cement materials with different water content. *Bulletin of the Chinese Ceramic Society*, Vol. 39, No. 7, 2020, pp. 2073–2078.
- [18] Richardson, I. G. and G. W. Groves. Microstructure and microanalysis of hardened ordinary Portland cement pastes. *Journal of Materials science*, Vol. 28, No. 1, 1993, pp. 265–277.

- [19] Hou, D., T. Yang, J. Tang, and S. Li. Reactive force-field molecular dynamics study on graphene oxide reinforced cement composite: functional group de-protonation, interfacial bonding and strengthening mechanism. *Physical Chemistry Chemical Physics*, Vol. 20, No. 13, 2018, pp. 8773–8789.
- [20] Manzano, H., S. Moeini, F. Marinelli, A. C. T. Van Duin, F. J. Ulm, and R. J. M. Pellenq. Confined water dissociation in microporous defective silicates: mechanism, dipole distribution, and impact on substrate properties. *Journal of the American Chemical Society*, Vol. 134, No. 4, 2012, pp. 2208–2215.
- [21] Hou, D., J. Yu, J. Zhang, B. Dong, and M. Zhang. Research on the mechanism of hydrolysis and weakening of hydrated calcium silicate based on reaction force field molecular dynamics. *Journal of Hydraulic Engineering*, Vol. 52, No. 1, 2021, pp. 34–41.
- [22] Guo, K., H. Ma, and F. Yang. Micromechanical properties of GO-RC interfacial transition zone under freeze-thaw cycles. *Journal of building materials*, Vol. 23, No. 1, 2020, pp. 230–238.
- [23] Xiaoxuan, G. Molecular dynamics study on the mechanical properties of hydrated calcium silicate/graphene composites, Taiyuan University of Technology, Taiyuan, 2020.
- [24] Tao, D. Study on the nano-modification mechanism of cementbased materials, Harbin Institute of Technology, Harbin, 2019.
- [25] Yang, Z. Study on the microstructure and properties of calcium silicate hydrates based on molecular dynamics simulation, Southeast University, Nanking, 2018.
- [26] Zdeněk, S. Role of the glass phase in bioactive glass-ceramics. *Biomaterials*, Vol. 52, No. 12, 1992, pp. 254–263.
- [27] Tilocca, A. Structural models of bioactive glasses from molecular dynamics simulations. *Proceedings of the Royal Society A: Mathematical, Physical and Engineering Sciences*, Vol. 465, No. 2104, 2009, pp. 1003–1027.

- [28] Cheng, Z., S. Yang, and X. Yuan. Research progress of graphene and its derivatives blending cement-based materials. *Journal of Composite Materials*, Vol. 38, No. 2, 2021, pp. 339–360.
- [29] Sun, H., L. Zhang, Q. Yang, Q. Liu, and M. Gao. Analysis of abnormal fluctuations in refractive index of CO₂ in the nearcritical region based on molecular dynamics simulation. *Chinese Journal of Power Engineering*, Vol. 41, No. 5, 2021, pp. 426–432.
- [30] Taylor, F. H. Cement chemistry, Vol. 20, No. 4, 2nd edn, Thomas Telford, UK, 1997, p. 335.
- [31] Zhao, Q., Z. Wang, X. Xu, C. Cui, S. Zhang, and X. Ding. Current research on the crystal structure, thermal behavior and synthesis of tobermorillonite. *Journal of the Chinese Ceramic Society*, Vol. 48, No. 10, 2020, pp. 1536–1551.
- [32] Lin, S., C. Ionescu, K. J. Pike, M. E. Smith, and J. R. Jones. Nanostructure evolution and calcium distribution in sol-gel derived bioactive glass. *Journal of Materials Chemistry*, Vol. 19, No. 9, 2009, pp. 1276–1282.
- [33] Martel, L., M. Allix, F. Millot, V. Sarou-Kanian, E. Véron, S. Ory, et al. Controlling the size of nanodomains in calcium aluminosilicate glasses. *The Journal of Physical Chemistry C*, Vol. 115, No. 39, 2011, pp. 18935–18945.
- [34] Mujah, D. Compressive strength and chloride resistance of grout containing ground palm oil fuel ash. *Journal of cleaner production*, Vol. 112, 2016, pp. 712–722.
- [35] Lv, S., Y. Ma, C. Qiu, T. Sun, J. Liu, and Q. Zhou. Effect of graphene oxide nanosheets of microstructure and mechanical properties of cement composites. *Construction and building* materials, Vol. 49, 2013, pp. 121–127.
- [36] Jiannan, T. Numerical analysis of the mechanical properties of graphene oxide cement-based materials. *Concrete*, Vol. 9, 2020, pp. 88–91.